JOURNAL OF THE MECHANICAL BEHAVIOR OF BIOMEDICAL MATERIALS 36 (2014) 71–81

Available online at www.sciencedirect.com

ScienceDirect

www.elsevier.com/locate/jmbbm


Research Paper

# A new class of bio-composite materials of unique collagen fibers

Mirit Sharabi[a,b], Yael Mandelberg[c], Dafna Benayahu[b], Yehuda Benayahu[c], Abdussalam Azem[d], Rami Haj-Ali[a,*]

[a]School of Mechanical Engineering, The Fleischman Faculty of Engineering, Tel Aviv University, Tel Aviv 69978, Israel
[b]Department of Cell And Developmental Biology, Sackler School of Medicine, Tel Aviv University, Tel Aviv 69978, Israel
[c]Department of Zoology, George S. Wise Faculty of Life Sciences, Tel Aviv University, Tel Aviv 69978, Israel
[d]Department of Biochemistry and Molecular Biology, George S. Wise Faculty of Life Sciences, Tel Aviv University, Tel Aviv 69978, Israel

ARTICLE INFO

*Article history:*
Received 5 February 2014
Received in revised form
8 April 2014
Accepted 10 April 2014
Available online 18 April 2014

*Keywords:*
Collagen
Bio-composite
Soft tissue
Mechanical behavior
Hyperelastic

ABSTRACT

A novel collagen-based bio-composite was constructed from micro-crimped long collagen fiber bundles extracted from a soft coral embedded in alginate hydrogel matrix. The mechanical features of this bio-composite were studied for different fiber fractions and in longitudinal and transverse loading modes. The tensile modulus of the alginate hydrogel was 0.60±0.35 MPa and in longitudinal collagen-reinforced construct it increased up to 9.71±2.80 for 50% fiber fraction. Ultimate tensile strength was elevated from 0.08±0.04 MPa in matrix up to 1.21±0.29 for fiber fraction of 30%. The bio-composite demonstrated hyperelastic behavior similar to human native tissues. Additionally, a dedicated constitutive material model was developed to enable the prediction of the longitudinal mechanical behavior of the bio-composite. These findings will allow tailor-designed mechanical properties with a quantitatively controlled amount of fibers and their designed spatial arrangement. This unique bio-composite has the potential to be used for a wide range of engineered soft tissues.



## 1. Introduction

Soft tissues can be viewed as an assembly of biomaterials that form a variety of heterogeneous material systems, each intended for distinct biological and mechanical environment.

Today, it is still a challenging task to develop scaffold for soft tissue repair that will provide appropriate mimic of native tissues. Tailoring the mechanical behavior of engineered tissues is essential, such as their resistance and response when subjected to tensile or compression loading forces, since mechanically unfitted implant may cause damage to the host tissue (Hollister, 2009). For instance, discrepancies in aortic tissue implant lead to differences in the local mechanical properties which ultimately can cause pseudo-aneurysm or intimal hyperplasia (Tremblay et al., 2009). These pathologies evolve due to local remodeling of the host tissue and are caused in part due to mechanical stress concentration.

*Corresponding author. Tel.: +972 3 640 8207.
*E-mail address:* rami98@tau.ac.il (R. Haj-Ali).

http://dx.doi.org/10.1016/j.jmbbm.2014.04.008
1751-6161/

Collagen is a structural protein that functions as mechanical support and load bearing element in tissues. In addition, it holds a variety of biological functions as cell–matrix interactions and binder for other proteins (as fibronection, decorin, etc.) to promote essential cellular functions (Parenteau-Bareil et al., 2010). Thus, collagen-based materials serve as initiating basis in tissue engineering (Bowles et al., 2010; Caves et al., 2010a; Gentleman et al., 2003; Hahn et al., 2006; Parenteau-Bareil et al., 2010; Rafat et al., 2008; Zeugolis et al., 2008). Mammalian sourced collagens have been widely explored to produce scaffolds. In order to use them as biomaterials they demand processing and de-cellularization from tissues' associated cells, such processing may leave collagen with immunogenic residues. When they are not completely removed these residues can lead to inflammatory reactions (Fitzpatrick et al., 2010; Liao et al., 2008; Parenteau-Bareil et al., 2010). Additionally, processing procedures can reduce graft strength up to two orders of magnitude relative to the native collagen (Chen et al., 2008).

A variety of collagen strengthening methods, fiber formation and crosslinking techniques have been designed in order to construct the complex structure of native collagen or to develop suitable substitutes (Caves et al., 2010b; Kumbar et al., 2008; Tamayol et al., 2013; Telemeco et al., 2005; Zeugolis et al., 2008). Alternative collagen sources have been explored including marine (Benayahu et al., 2011; Jeong et al., 2007; Songa et al., 2006) and human recombinant collagen expressed in plants (Ruggiero et al., 2000). Achieving pure and strong collagen fibers as biomaterials is required for the various biomedical applications, combining strength and biocompatibility. The latter fibers can be embedded in matrix binders as layers or laminated in order to construct collagen-reinforced composites for tissue regeneration and repair. These matrices can be hydrogels as chitosan (Pok et al., 2013; Wright et al., 2012), gelatin (Pok et al., 2013) or gellan gum (Thorvaldsson et al., 2013). Such bio-composite might be considered advantageous since the hydrogel matrix provides soft and aqueous surroundings that benefit the resident cells, diffusion processes and three-dimensional structure, similar to the native proteoglycans and the stiff fibers allow mechanical robustness and structural strength (Pok et al., 2013; Thorvaldsson et al., 2013). Fiber reinforced bio-composites have recently been developed to provide desired mechanical and biological features for tissue-repair applications including cartilage (Wright et al., 2012), abdominal wall (Caves et al., 2011), blood vessels (Caves et al., 2010a; Kumar et al., 2013), cardiac tissue (Pok et al., 2013) and nucleus pulpous (Thorvaldsson et al., 2013).

Herein, we report the fabrication of a novel all-natural bio-composite material system based on unique long collagen fibers extracted from a soft coral (Benayahu et al., 2011) reinforcing an alginate hydrogel matrix (Haj-Ali et al., 2013). The fibers were isolated from the soft coral as folded bundles and when slightly stretched during extraction they reached up to 20 cm in length. The fiber bundles in their natural surroundings are heavily coiled in the coral mesenteries of the polyp (Benayahu et al., 2011). Vast morphological and biochemical analyses indicated that the fibers are resembled to type I collagen (Benayahu et al., 2011) by their amino acid composition as found by Nuclear Magnetic Resonance spectroscopy (NMR) and by mass using mass spectroscopy (MS). Transmission electron microscopy (TEM) and Masson trichrome staining also strengthen this determination. However, differences between the collagen from soft coral and mammalian sources do exist, such as the higher melting temperature of the coral collagen and its bundle form of nested helical packing. These collagen fibers present melting temperature of 68 °C that suggests high natural cross-linking degree. The fibers possess tensile strength of 39–59 MPa and stiffness of 0.34–0.54 GPa on isolated fibers (Benayahu et al., 2011). These unique collagen fibers consist of natural micro-crimping (coiling) which is essential for hyperelastic mechanical behavior of soft tissues (Caves et al., 2010c; Holzapfel, 2001). The collagen fibers are also biocompatible and shown to support cell growth both *in vivo* and *in vitro* studies (Benayahu et al., 2011).

In the current study, the soft coral fibers were aligned in specified controlled orientation to provide preferential mechanical properties, such as anisotropic stiffness and tensile strength. These properties can be tailored and controlled based on the volume of fibers ($V_f$) used in the reinforcement of the alginate matrix. The alginate hydrogel was derived from marine algae and has been widely used for biomedical applications (Ertesvig and Valla, 1998; Kuo and Ma, 2001; Lee and Mooney, 2012).

## 2. Materials and methods

### 2.1. Isolation and purification of collagen fibers

Soft coral *Sarcophyton* (Benayahu et al., 2011) was kept frozen pre-reaping and defrosted before fiber extraction. A piece of colony was reaped to expose the fibers and the exposed fibers were physically pooled out from the soft coral (Fig. 1a). They manually spun around thin U-shaped stainless steel wire to create unidirectional, straight and organized array of fiber bundles (Fig. 1b). The aligned fibers were carefully washed several times in water and then with 70% ethanol.

### 2.2. Bio-composite fabrication

The spun fiber bundles (Fig. 2a) were inserted to a dialysis membrane (6000–8000 MWCO, Spectra Por) together with 3 ml Sodium alginate solution (3% w/v in DDW, Protanal LF 10-60, FMC BioPolymer) (Fig. 2b). The alginate and collagen were cross-linked with a 45 mM EDC [*N*-(3-Dimethylaminopropyl)-*N*′-ethylcarbodiimide hydrochloride, Sigma-Aldrich] – NHS (*N*-Hydroxy-succinimide, Sigma-Aldrich) (Fig. 2d). The membrane was sealed, flattened and soaked in 0.1 M $CaCl_2$ (Merck) solution to enable ionic gelation of alginate hydrogel through diffusion for 48 h at room temperature (Fig. 2c). Then, the bio-composite was removed from membrane and frame (Fig. 2e). Matrix fabrication was conducted as for the bio-composite, excluding the fiber insertion and crosslinking.

### 2.3. Fibers quantification and orientation

The arranged fibers were photographed on a dark background (Samsung camera, 8 Megapixels) and images were processed

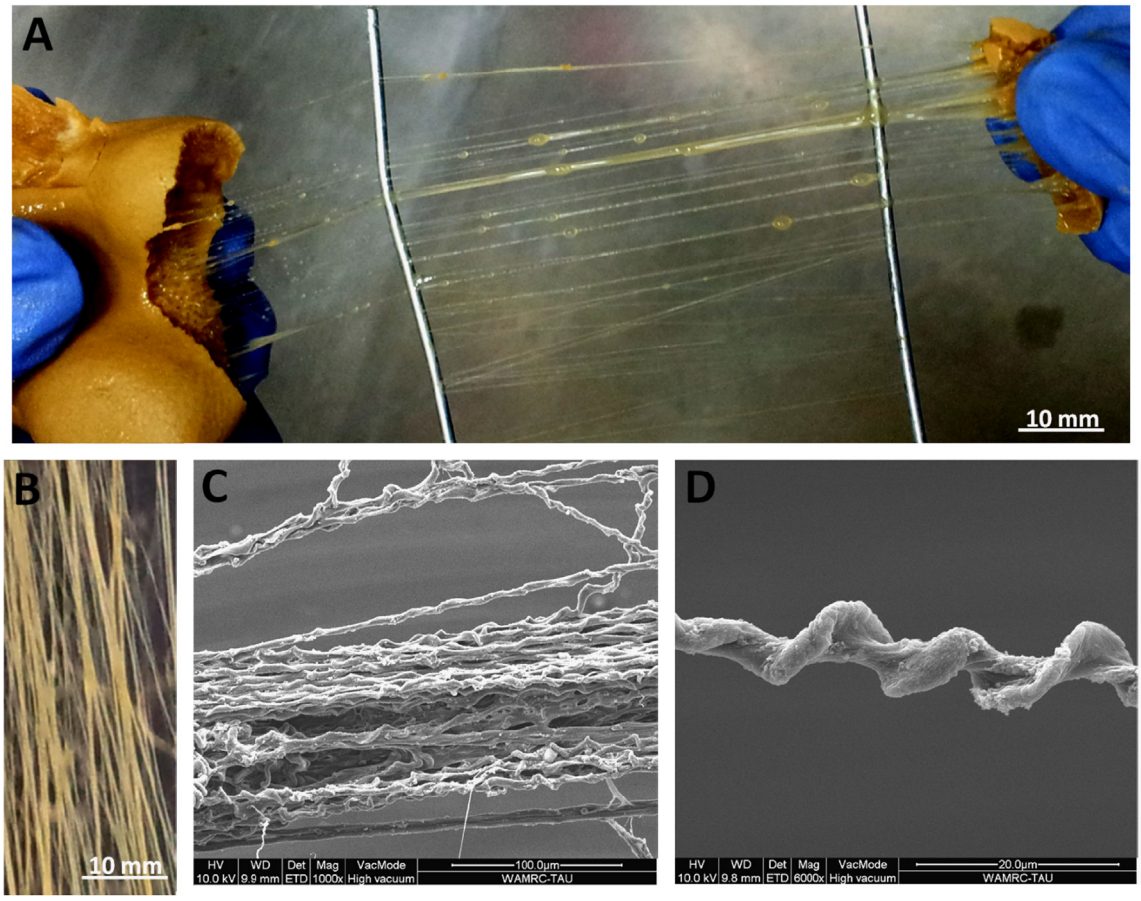


**Fig. 1 – Coral collagen fibers. (A) Bundles of collagen fibers extracted from torn apart Sarcophyton soft coral colony, streched fibers still connected to each piece. (B) Collagen fibers aligned in unidirectional orientation. (C) SEM image of coral collagen fibers (× 1000). (D) SEM image of isolated fiber: fibers are naturaly coiled (microcrimped) in spring-like structure (× 6000).**

to binary images (Fig. 3a and b). Fiber fraction was determined by calculating the percentage of white pixels (fibers) from the dark background using Matlab program (Fig. 3c). The 2D fiber fraction was divided in the normalized thickness of the bio-composite. The preferred orientation was captured using Fast Fourier transform (FFT) filter and bright pixels were quantified using Oval profile plug in (ImageJ, NIH) (Fig. 3d and e).

### 2.4. *Scanning electron microscopy*

Examination of the microstructural features of the collagen fibers and bio-composites was conducted by SEM (Quanta 200 FEG Environmental Scanning Electron Microscope). The samples were fixed in 4% glutaraldehyde and dehydrated through a graded series of ethanol up to 100%. The samples were sputtered with gold/palladium alloy and then examined with SEM at high vacuum.

### 2.5. *Mechanical testing*

#### 2.5.1. *Mechanical behavior measurements*

Tensile testing was performed on Instron machine model 5582 with Bluehill 2 operating software and 100 N load cell under static strain rate using displacement control mode. The samples were gripped with Instron Screw Side Action grips; gripping zone was 10 mm in every side in order to prevent slipping of the sample. The total dimensions of rectangular shaped samples without the gripping zones were about 15 mm (width) × 25 mm (gage length) × 1 mm (thickness). The DIC technique was applied initially to examine the manufacturing and material integrating. It was also used as an optical extensometer in order to extract the average strain values. This method was also used to compare with the average strains read by the loading frame. The differences found were extremely small for the entire loading history up to failure. Samples were preconditioned up to 10% strain. The results were following 3–16 cycles did not show significant differences in the stress–strain behavior and the hysteresis loops. At least three cycles of loading were applied in the post-conditioning to each sample before reporting its representative stress–strain behavior.

Forty-six samples were tested: 24 samples were stretched in the fibers' direction (12 of them were used for calibration of the proposed uniaxial model) and 12 samples were stretched perpendicular to the fibers directions (transverse samples) in addition to 10 matrix samples (Alginate hydrogel only). A model verification set was subjected to 10% strain after preconditioning; all the other samples were preconditioned and then stretched to failure.

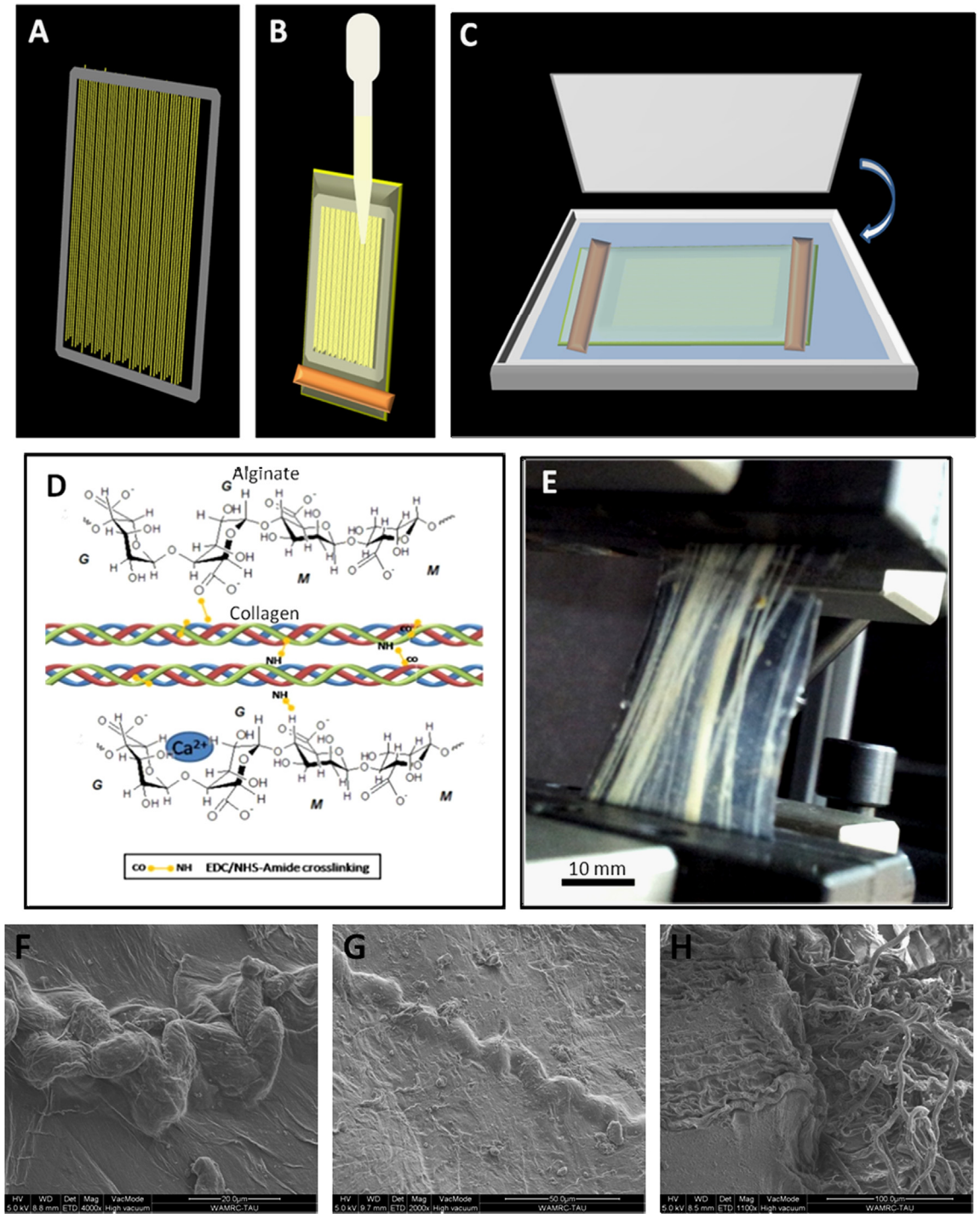


**Fig. 2 – Illustration of collagen-based bio-composite fabrication. (A) Unidirectional collagen fibers arranged on rectangular frame. (B) Alginate solution injection to the oriented collagen fibers. (C) Gelation of alginate using $Ca^{2+}$ ions. (D) Crosslinking of the bio-composite using EDC-NHS and $Ca^{2+}$ ions- molecular illustration. (E) Unidirectional collagen fibers embedded in alginate hydrogel matrix. SEM images of fibers embedded bio-composites upper view (G, H) and cross-section view (F).**

2.5.2. *Mechanical uniformity of bio-composite*

Digital Image Correlation (DIC) measurements and analysis were employed using LaVision 2D StrainMaster system with 12-bit CCD digital camera and DaVis 7.4 software (Sasson et al., 2012; Sutton et al., 1983, 2009). The latter included a 12-bit CCD digital camera, analog to digital converter, for load data synchronization between the Instron machine, and the DaVis 7.4 software. Test data was recorded using a camera rate of 3 Hz and was synchronized with the loading frame measurements. Prior sample preparation included spraying a powder mixture using air flow on surface of the bio-composite in order to achieve random-speckle and a good contrast for the DIC post-processing algorithm. The native composite was transparent (except for the aligned fibers),

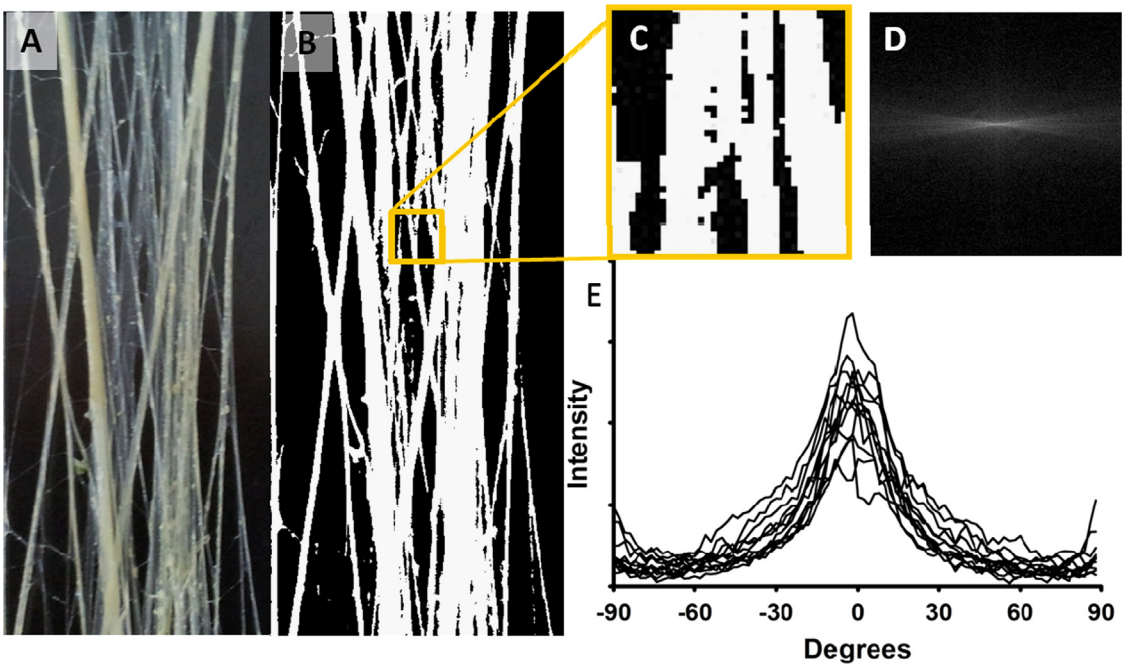


**Fig. 3 – Fiber volume fraction and orientation. (A) Image of arranged unidirectional collagen fibers. (B) Binary image of arranged collagen fibers. (C) Determination of fiber fraction from white pixels percentage from total pixels. (D) FFT image of arranged unidirectional collagen fibers. (E) FFT analysis of all bio-composites presented as intensity, all the fibers are arranged in $0^0$ with the vertical axis.**

therefore, the powder included a mixture of both black and white particles in the form of graphite, average size 4–6 μm, and alumina, averaged size 0.3 μm, respectively.

### 2.6. *Longitudinal bio-composite modeling*

Mooney–Rivlin hyperelastic strain-energy density function was fitted to the experimental data.

The strain energy density can be expressed by

$$W = C_{10}(I_1 - 3) + C_{01}(I_2 - 3) + \frac{1}{D_1}(j-1)^2 \quad (1)$$

$I_1$ and $I_2$ are the first and second strain invariants, respectively, of the left Cauchy–Green strain tensor. The strain energy density function is composed from two parts. The first defines the incompressible part of the function using the first and second invariants, while the second part describes the compressible behavior using the third strain invariant. Under the assumptions that the material is isotropic (longitudinal composites limited to uniaxial loading) and incompressible (due to the hydrogel); the stress–strain relation is derived from the strain energy density function of the simplified Mooney–Rivlin equation by

$$\sigma_e = \frac{\partial W}{\partial \lambda} = \frac{2}{1+e}\left((1+e)^2 - \frac{1}{1+e}\right)\left(C_{10} + \frac{C_{01}}{1+e}\right) \quad (2)$$

The constants $C_{ij}$ are determined based on experimental data (alginate samples and a test set of bio-composite samples) using least squared curve fitting of Abaqus 6.9 (SIMULIA) software.

### 2.7. *Longitudinal bio-composite predictive model*

The material behavior was assumed to be isotropic and hyperelastic; therefore, an existing strain energy function for hyperelastic materials was used. This derivation enabled us to model collagen fiber and alginate separately by applying stress–strain relationships of each component accordingly. The unidirectional response of the bio-composite was assumed as a parallel arrangement of springs representing the collagen fibers and alginate matrix. Fig. 7a presents illustrate of this parallel arrangement. Thus, for a given applied strain, the effective stress was the weighted stress sum of the two constituents (Eq. (3)) and the strains of the matrix, fibers and bio-composite were equal (Eq. (4)). Therefore the well-known rule of mixtures can be applied in its simple version.

$$\sigma_{composite} = V_{matrix}\sigma_{matrix} + V_{fiber}\sigma_{fiber} \quad (3)$$

The compatibility of the strains in the matrix and fiber constituents can be written using parallel analogy of springs as

$$\varepsilon_{composite} = \varepsilon_{matrix} = \varepsilon_{fiber} \quad (4)$$

At first, rule of mixtures was applied for the calibration of the theoretic value of the equivalent fiber based on matrix and $V_f$=50% and $V_f$=25% samples up to 10% strain (in order to exclude damage influence). Later, different combinations of $V_f$=0% (matrix) and $V_f$=100% (equivalent fiber) were used to predict the behavior of bio-composites with other fiber fractions. Validation set with different fiber fractions was used to validate the accuracy of the model up to failure.

### 2.8. Statistical analysis

Mean and standard deviation were obtained for all measurements. Comparisons were made using ANOVA for multiple comparisons, with Tukey post hoc analysis for parametric data. Paired and one sample t-tests were performed in order to compare the experimental Mooney–Rivlin coefficients to the predictive value. A value of $p<0.05$ was considered statistically significant.

## 3. Results

### 3.1. Fabrication of matrix and bio-composite

The matrix and bio-composites fabrication process yielded uniform samples without any visible voids or cavities in the macro-scale. Fig. 4 is a representative DIC image showing a good uniformity of this specific sample. While several samples were subjected to DIC testing to ensure the repeatability of material, no rigorous optimization of the fabrication process was conducted. Thus some of the above defects may be contained in our samples. The Calcium ions diffused into the dialysis membrane, creating uniform hydrogel with controlled geometry which enabled tensile testing of the hydrogels. The hydrogel width was $15.73\pm2.53$ mm, the gage length was $23.56\pm2.06$ mm and thickness of $1.49\pm0.66$ mm. The bio-composite resulted in encapsulated pre-determined fiber arrangement of the collagen fibers embedded in a soft alginate hydrogel (Fig. 2f–h). The hydrogel matrix provided aqueous surroundings for the collagen fibers, preventing their dehydration during tensile measurements. The composites featured width of $10.17\pm3.95$ mm, gage length of $19.72\pm4.71$ mm and thickness of $0.84\pm0.37$ mm ($n=36$). Fiber fraction was ranged between 0.05–0.59. Fiber orientation measurements are presented in Fig. 3(e) by FFT measurements, confirming that the main direction of the fibers is $0^0$ with the vertical axis.

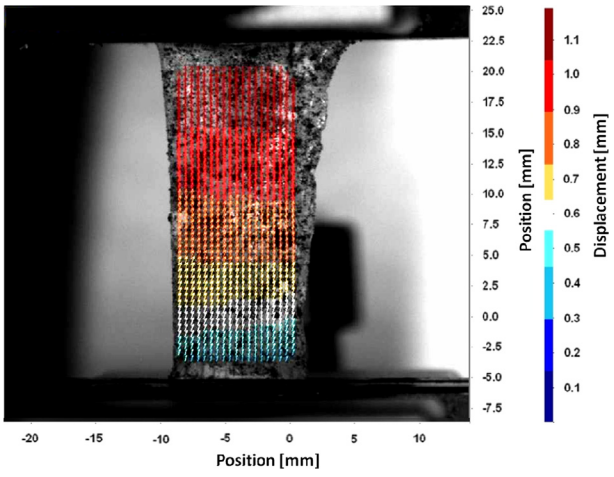


**Fig. 4 – Representative image of Bio-composite linear displacement field at applied remote at 5% tensile strain. The uniform linear displacement field of the bio-composite was determined using the DIC (digital image correlation) method.**

### 3.2. Digital image correlation (DIC) measurements of bio-composite

The mechanical integrity of the bio-composite was examined and in order to rule out slipping between the fibers and the matrix, DIC technique was applied during the tensile measurements. Fig. 4 exhibits representative image of linear displacement field revealed on the surface of the bio-composite during a tensile test. The measurements maintained for three repeated tensile loading cycles and up to 10% strain level. This finding indicates a spatial uniformity of the mechanical properties within the bio-composite and its homogeneity and integrity.

### 3.3. Mechanical behavior of the bio-composite

The bio-composites demonstrated a hyperelastic behavior with large deformations. The non-linear stress–strain behavior is characterized with relatively low stress response at the beginning of the loading, followed by increased stiffness (Figs. 7 and 8). Longitudinal bio-composites are characterized by full range hyperelasticity, when fiber fraction increased less damage is caused to the matrix (Fig. 7). However, transverse samples which are matrix dominated are more subjected to damage. Hence, hyperelastic behavior is observed up to 10% strain (Fig. 8).

All mechanical properties are presented for true stress–strains. Failure properties are described in Fig. 5, all the bio-composites demonstrated higher strength than the matrix ($0.08\pm0.04$ MPa at $0.18\pm0.06$ strain). Longitudinal composites demonstrated higher strength than transverse composites for all tested fiber fractions. The ultimate strength of bio-composites was changed between the different fiber fractions, the higher the fraction, the larger the tensile strength for longitudinal and transverse samples (for longitudinal: $V_f=0.14-0.50\pm0.29$ MPa at $0.18\pm0.04$ strain ($n=4$), for $V_f=0.21-0.69\pm0.18$ MPa at $0.19\pm0.04$ strain ($n=5$) and for $V_f=0.30-1.21\pm0.29$ MPa at $0.20\pm0.03$ ($n=3$) strain, for transverse composites with $V_f=0.07-0.11\pm0.06$ MPa at $0.17\pm0.04$ strain ($n=6$) and $V_f=0.22-0.26\pm0.09$ MPa at $0.19\pm0.03$ strain ($n=6$), as presented in Fig. 5). Differences in the failure strains were not significant between the groups or matrix.

In order to simplify the hyperelastic stress–strain behavior and to calculate the stiffness, the non-linear relation can be idealized as bilinear with two slopes, i.e., toe region and linear region as known for other soft tissues (Holzapfel, 2001). Tangential stiffness was calculated separately for the toe and linear region as described in Fig. 6(a). First derivative of stress–strain curves was calculated and the tangential stiffness was recorded at strain levels of 3% and 9%, respectively. The second derivative of the region after the toe region (from 5% to 10%) is approximately constant, Thus, allow to define the second stiffness (9% strain) as linear region. The stiffness of the composites as a function of the fiber volume fraction in the toe region and linear region is presented in Fig. 5(c and d). The linear region was significantly stiffer than the toe region for longitudinal bio-composites with $V_f>0.2$. Longitudinal bio-composites were significantly stiffer from the matrix in the linear region (ANOVA,$p<0.001$). Longitudinal composites

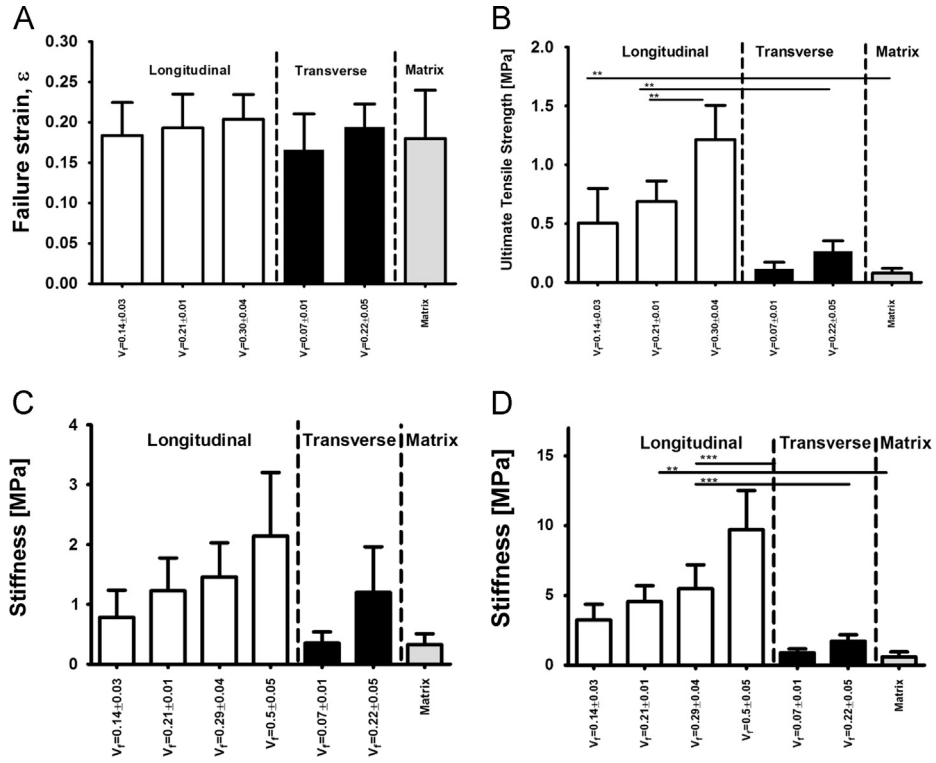


**Fig. 5 – Mechanical properties of the bio-composites by fiber volume for longitudinal (white), transverse (black) bio-composites and matrix (gray).(A) Failure strain. (B) Ultimate tensile strength. (C) Tangential stiffness in toe region (3% strain). (D) Tangential stiffness in linear region (9% strain).**

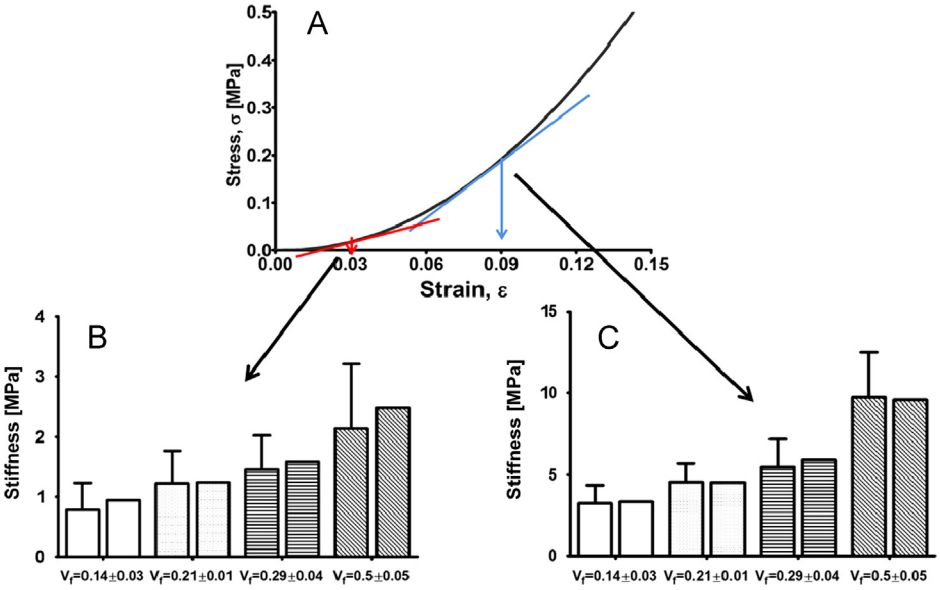


**Fig. 6 – Stiffness determination. In order to simplify the materials behaviors' stiffness, the hyperelastic stress–strain curve was simplified to bi-linear curve. (A) Example for bilinear fitting for unidirectional bio-composites. Tangential stiffnesses were calculated for 3% and 9% strains and presented as low and high young modulus, respectively. Predicted values were calculated for the averaged fiber volume. Measured values (with SD) presented in the left columns, predicted- in the right. (B) Tangential stiffness in the toe region at 3% strain level. (C) Tangential stiffness in the linear region at 9% strain level.**

with $V_f=0.2$ were significantly stiffer than transverse composites with the same fiber fraction (ANOVA, $p<0.0001$). The differences between the groups were not significant for the toe region or for $V_f=0.14$.

### 3.4. *Predictive longitudinal composite model*

Test data ($n=12$) was used for calibration of the Mooney–Rivlin hyperelastic constitutive model. The Mooney–Rivlin

**Table 1 – Predicted and experimental Mooney–Rivlin coefficients for different fiber fractions.**

| Material system (model) | $c_{10}$= | $c_{01}$= | Material system (experimental) | $c_{10}$= | $c_{01}$= | Material system (experimental) | $c_{10}$= | $c_{01}$= |
|---|---|---|---|---|---|---|---|---|
| Experimental matrix | 0.77 | −0.76 | $V_f$=34.9% | 6.29 | −6.34 | $V_f$=58.5% | 7.65 | −7.77 |
| Predicted $V_f$=10% | 2.52 | −2.52 | $V_f$=28.1% | 7.51 | −7.59 | $V_f$=53.2% | 11.42 | −11.51 |
| *Predicted $V_f$=25% | 5.28 | −5.32 | $V_f$=26.6% | 3.36 | −3.40 | $V_f$=47.9% | 10.05 | −10.18 |
| *Predicted $V_f$=50% | 9.58 | −9.69 | $V_f$=22.7% | 5.89 | −5.95 | $V_f$=47.7% | 6.29 | −6.35 |
| Predicted $V_f$=75% | 13.84 | −14.00 | $V_f$=20.5% | 4.99 | −5.03 | $V_f$=46.4% | 7.40 | −7.49 |
| Predicted $V_f$=100% | 18.19 | −18.42 | $V_f$=19.8% | 4.50 | −4.51 | $V_f$=44.9% | 12.29 | −12.38 |
| | | | *$V_f$ average=25% | 5.42 | −5.47 | *$V_f$ Average=50% | 9.18 | −9.28 |

* Significant difference in combined DEET between FA and FB/FC.

constants (described in Eqs. (1) and (2)) of the fitted experimental results are presented in Table 1.

The samples (bio-composite and matrix) were fitted to Mooney–Rivlin hyperelastic material with two coefficients (Table 1). Rule of mixtures was used to calibrate (Eq. (3)) the effective properties of equivalent fiber ($V_f$=100%) as the average of 12 different composites ($V_f$=25±5.6, $n$=6 and $V_f$=50±5.1%, $n$=6). The predictive coefficients values in Table 1 were calculated using the limit cases of matrix ($V_f$=0%) and equivalent fiber ($V_f$=100%). The hyperelastic mechanical behavior up to 10% strain and the limit cases are presented in Fig. 7(a). Additional fiber fractions can be calculated using the model. The prediction of the proposed model for the verification cases of $V_f$=25% and $V_f$=50% showed good correlation with the correspond experimental results (Table 1).

Validation set was fabricated to test the model up to failure in additional fiber fractions, Fig. 7(b) demonstrates the model compatibility to the experimental results.

In order to define the stiffening effect on different fiber fractions, the elasticity modulus was calculated separately for the toe and linear regions (as described above) as a function of the fiber volume fraction, stiffness was calculated for all longitudinal samples (calibration and validation sets). Fig. 6(b and c) compares the predictive and experimental stiffness, the differences between the model and experiments were not significant. Thus, the model can give good approximation for the longitudinal bio-composites in varied fiber fractions.

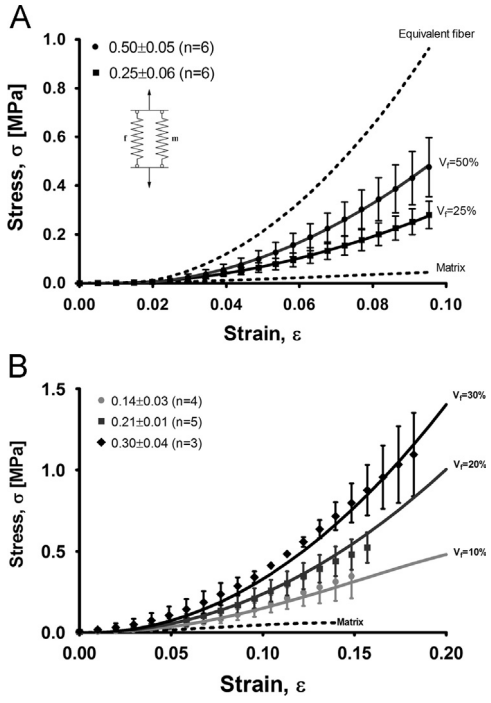


**Fig. 7 – Hyperelastic tensile stress–strain curves of collagen bio-composites for different fiber volume fractions (FVFs). (A) Calibration of the micromechanical model for the in situ fiber hyperelastic properties using matrix-alone and test results for two cases of FVFs up to 10% strain. The experimental values were generated from repeated uniaxial tests ($n$=6). (B) Model predictions and validation for bio-composites having different FVFs in the full range of imposed strain magnitudes (up to failure). Validation set included three groups with different fractions: $V_f$=0.14 ($n$=4), $V_f$=0.21 ($n$=5),$V_f$=0.30 ($n$=3).**

## 4. Discussion

In the current study, a novel and natural bio-composite based on collagen fibers reinforced alginate hydrogel was designed, fabricated (Fig. 2) and mechanically tested in longitudinal and transverse modes. The effective mechanical behavior of the bio-composite is non-linear and hyperelastic, similar to native soft tissues (Fung, 1967). Bio-composites were constructed with varied fractions of collagen fibers, all aligned unidirectional and verified by FFT filter (Fig. 3e). DIC measurements presented linear displacement field (Fig. 4), verifying the binding between the fibers and the matrix and indicating a uniform composite material system. This finding is also repeated after several loading cycles. It is suggested that the adhesion between the matrix and fibers is covalent binding based on the carbodiimide chemistry applied during the preparation of the bio-composite and/or to non-covalent interactions as ionic and Van-der Waals interactions since both charged molecules are involved.

Mechanical properties of isolated fibers are larger in an order of magnitude than connective tissues. However, the longitudinal bio-composite demonstrated 1–2 orders of magnitude less in stiffness (2–13 MPa) and strength (0.4–1.5 MPa),

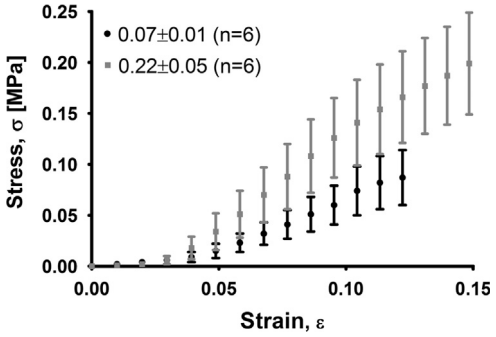


**Fig. 8 – Mechanical behavior of transverse bio-composites for fiber fractions of 0.07 ($n=6$) and 0.22 ($n=6$).**

depends on the volume fraction, than the isolated coral fibers (0.34–0.54 GPa and 39–59 MPa, respectively). The stiffness and strength of the matrix and fibers differ in about three orders of magnitude, 0.6 MPa and 0.08 MPa, respectively. This allows for a wider degree of freedom for designing and manufacturing the bio-composite for pre-specified elastic properties. The equivalent fiber properties are lower than the actual fiber due to the cross-sectional area which is different for the equivalent and "real" fiber.

When stretching the bio-composites' in the fibers direction (longitudinal) strength was larger than in the transverse direction due to the load that the collagen fibers bear. The differences in stiffness were significant in the linear region, but not in the toe region, where all samples are matrix dominated. In higher strains, the distribution of results is wider, since matrix exhibits damage behavior and the composite exhibits a strong stiffness reduction. The mechanical damage behavior cannot be predicted by the simplified model.

The non-linear stress–strain behavior can be considered as a combination of two linear curves of the toe and linear regions. Suggested explanation for the longitudinal composites for this behavior lies in the structure–function relation; the toe regions' low stiffness can be attributed to straightening the collagen fiber micro-crimping (Fig. 1c and d), in this stage of the tensile behavior of the collagen fibers remain loose and unable to contribute notably to the overall performance. Thus, the reaction is matrix dominated. However, in the linear region the significantly higher stiffness is associated with stretching of the straight fibers (Fratzl et al., 1997; Holzapfel, 2001), where the fibers carry load and dominate the mechanical reaction. This behavior is characteristic of soft tissues due to the presence of collagen (Holzapfel, 2001). In the transverse composites, when the load is not in the fibers direction, the entire behavior is matrix dominated and the composites exhibited matrix damage.

The novel collagen bio-composite when subjected to axial load demonstrated significantly stiffer and stronger behavior compared to the matrix alone material (Figs. 5 and 7). Moreover, increasing fiber fraction resulted in proportional stiffening. This finding supports our use of parallel spring analogy for nonlinear mechanical constitutive model. Thus the volume fractions along with aligned orientation to the loading direction have greater influence on the overall material response. In the toe region, since the stress is low, the fiber fraction has relatively low influence compared to the linear region (Fig. 5c and d).

The coral fibers, as native collagen fibers, are micro-crimped (coiled) fibers (Fig. 1d) that forming tissue-like structure when embedded in a matrix. This new feature is unique in biomaterials and allows tissue contraction (Fleischer et al., 2013) and can facilitate load-shielding of embedded cells by sliding between these three dimensional coiled fibers (Thorpe et al., 2013). Dedicated technologies have developed for creating this kind of waved or "spring like" fibers which are essential for soft tissues mimicking (Caves et al., 2010c; Fleischer et al., 2013). These synthetic wavy fibers were embedded in elastin matrix (Caves et al., 2010c). The waviness increased the maximum deformation and reduced the stiffness. Their ultimate strength was similar to our results (1–2 MPa). However, Collagen SEM images (Fig. 1c and d) imply on higher order of crimping in our coral collagen (3D), which is a challenging task to achieve synthetically.

Fiber reinforced bio-composites are developed for varied biomedical applications (Caves et al., 2010a, 2011; Kumar et al., 2013; Pok et al., 2013; Thorvaldsson et al., 2013; Wright et al., 2012) most of them were tested for compression loads and little is known about tailoring their mechanical properties. The influence of different fiber fractions and orientations were examined on the composite material; increasing fiber fraction and reducing the angle to the loading direction have strengthened the composite (Caves et al., 2011). However, we did not found any reference for bio-engineered composite with the ability to computationally predict the mechanical behavior, and hence to tailor the material by tissue needs.

Both the matrix and the collagen composite revealed hyperelastic behavior and were modeled by Mooney–Rivlin hyperelastic energy potentials. The predicted results from this simplified nonlinear uniaxial model, allowed examining the behavior of bio-composites with additional fiber fractions.

We calculated a Young modulus from the linear region of the stress–strain curve after the toe region (as reviewed by McKee et al. (2011)) and often used to characterize hyperelastic soft tissues. Therefore these values can be compared to the current bio-composite. The measured stiffness values in the 14–21% fiber fraction range ($3.24\pm1.12$ MPa and $4.56\pm1.14$ MPa, respectively) within the linear region, match native tissues as sclera (~2.0 MPa), cornea (~2.7 MPa), artery and veins (~3.0 MPa) (McKee et al., 2011).

The experimental strength of the longitudinal bio-composite in $V_f=29\%$ ($1.21\pm0.29$ MPa) is compatible with the Adventitia layer of coronary artery $1.4\pm0.6$ and $1.3\pm0.7$ MPa for the circumferential and longitudinal directions, respectively (Holzapfel et al., 2005). Fiber fraction of 0.14 and 0.21 ($0.5\pm0.29$ MPa and $0.69\pm0.18$ MPa, respectively) is compatible with soft issues as aorta (0.3–0.8 MPa) (Holzapfel, 2001). Higher fiber fractions (as 70%) can be compatible with other soft tissues such as cornea with tensile strength of 3.3–4.4 MPa (Zeng et al., 2001). Although these tissues are composed of much complex structures and multidirectional orientations, the uniaxial bio-composite results can give good starting point for engineering a specific tissue using a unidirectional lamina in a multi-layer and multi-axial laminate. The axial orientation provides the upper bound of strength and stiffness, since fibers are in the loading direction.

The ability to predict the behavior of the composite and control its properties allows tailor design mechanical properties

based on the mechanical requirements of the natural tissues. Moreover, the ability to control and predict the density and distribution of the fibers may allow tailored design of more complex tissues which consist of regional changes in sub-areas of the tissues that resulted in regional changes in the mechanical properties, such as the stiffness changes with depth in the meniscus and cartilage (Lai and Levenston, 2010) or in the annulus fibrosus (Fujita et al., 1997). Orienting the laminates of axis from the loading direction will reduce the strength and allow fabrication of composite with compatible strength varied tissues as annulus fibrosus $0.30 \pm 0.16$(Ebara et al., 1996), and urinary bladder $0.27 \pm 0.14$ MPa (Dahms et al., 1998). Future work will engage in the mechanical behavior of oriented laminates, their composition and modeling in order to allow tailor-designed fabrication of specific complex tissue structure.

## 5. Limitations

The mechanical tests were performed under strain rates between 1 and 3 mm per minute assuming a static response of the material in this range. Therefore, the influence of the strain rate on the results was neglected. Collagen fibers are biological entities and thus contain some material variability. The latter emanates from non-uniform FVF distributions within the material, voids and other matrix–fiber bonding-cohesive and interphase properties. The current manual fabrication process has an additional effect on the distributions of the tested properties. The material behavior for the fiber and matrix constituents was assumed to be isotropic and hyperelastic since the current study is mainly concerned and limited to uniaxial loading. While the applied nonlinear rule of mixtures cannot be fully characterized as multi-axial and general material model, it offers a limited predictive model for the effective nonlinear axial response of the composite material when given the volume fractions and the nonlinear axial laws of the fiber and matrix. Finally, the analysis of the results and the proposed modeling approach did not take into account the damage response exhibited by the matrix for strain levels beyond 10%.

## 6. Conclusions

A new bio-composite material system is proposed, fabricated and mechanically investigated. It is based on long collagen fibers reinforcing an alginate hydrogel matrix. The bio-composite has hyperelastic behavior and can be tailored to yield mechanical properties similar to native tissues. The micro-structure of the fibers has unique nested coiled arrangement, at both the individual fiber and the bundle levels, which can explain its hyperelastic response. A new simplified nonlinear micromechanical material model is formulated for the bio-composite in its axial loading mode in order to predict the overall stress–strain relation from the in situ response of the fiber and matrix constituents. The prediction of the model has been verified against tested bio-composites with different fiber volume ratios.

## REFERENCES


Benayahu, Y., Benayahu, D., Kashman, Y., Rudi, A., Lanir, Y., Sela, I., Raz, E., 2011. US20110038914A1, Coral derived collagen and methods of farming same.

Bowles, R.D., Williams, R.M., Zipfel, W.R., Bonassar, L.J., 2010. Self-assembly of aligned tissue-engineered annulus fibrosus and intervertebral disc composite via collagen gel contraction. Tissue Eng. A 16, 1339–1348.

Caves, J.M., Cui, W., Wen, J., Kumar, V.A., Haller, C.A., Chaikof, E.L., 2011. Elastin-like protein matrix reinforced with collagen microfibers for soft tissue repair. Biomaterials 32, 5371–5379.

Caves, J.M., Kumar, V.A., Martinez, A.W., Kim, J., Ripberger, C.M., Haller, C.A., Chaikof, E.L., 2010a. The use of microfiber composites of elastin-like protein matrix reinforced with synthetic collagen in the design of vascular grafts. Biomaterials 31, 7175–7182.

Caves, J.M., Kumar, V.A., Wen, J., Cui, W., Martinez, A., Apkarian, R., Coats, J.E., Berland, K., Chaikof, E.L., 2010b. Fibrillogenesis in continuously spun synthetic collagen fiber. J. Biomed. Mater. Res. B 93, 24–38.

Caves, J.M., Kumar, V.A., Xu, W., Naik, N., Allen, M.G., Chaikof, E.L., 2010c. Microcrimped collagen fiber-elastin composites. Adv. Mater. 22, 2041–2044.

Chen, J., Xu, J., Wang, A., Zheng, M., 2008. Scaffolds for tendon and ligament repair. Expert Rev. Med. Devices 6, 61–73.

Dahms, S., Piechota, H., Dahiya, R., Lue, T., Tanagho, E., 1998. Composition and biomechanical properties of the bladder acellular matrix graft: comparative analysis in rat, pig and human. Br. J. Urol. 82, 411–419.

Ebara, S., Iatridis, J.C., Setton, L.A., Foster, R.J., Mow, V.C., Weidenbaum, M., 1996. Tensile properties of nondegenerate human lumbar anulus fibrosus. Spine 21, 452–461.

Ertesvig, H., Valla, S., 1998. Biosynthesis and applications of alginates. Polym. Degrad. Stab. 59, 85–91.

Fitzpatrick, J., Clark, P., Capaldi, F., 2010. Effect of decellularization protocol on the mechanical behavior of porcine descending aorta. Int. J. Biomater., 1–11.

Fleischer, S., Feiner, R., Shapira, A., Ji, J., Sui, X., Daniel Wagner, H., Dvir, T., 2013. Spring-like fibers for cardiac tissue engineering. Biomaterials 34, 8599–8606.

Fratzl, P., Misof, K., Zizak, I., 1997. Fibrillar structure and mechanical properties of collagen. J. Struct. Biol. 122, 119–122.

Fujita, Y., Duncan, N.A., Lotz, J.C., 1997. Radial tensile properties of the lumbar annulus fibrosus are site and degeneration dependent. J. Orthop. Res. 15 (6), 814–819.

Fung, Y., 1967. Elasticity of soft tissues in simple elongation. Am. J. Physiol.Leg. Content 213, 1532–1544.

Gentleman, E., Lay, A.N., Dickerson, D.A., Nauman, E.A., Livesay, G.A., Dee, K.C., 2003. Mechanical characterization of collagen fibers and scaffolds for tissue engineering. Biomaterials 24, 3805–3813.

Hahn, M.S., Teply, B.A., Stevens, M.M., Zeitels, S.M., Langer, R., 2006. Collagen composite hydrogels for vocal fold lamina propria restoration. Biomaterials 27, 1104–1109.

Haj-Ali, R., Benayahu, Y., Benayahu, D., Sasson-levi, A., Sharabi, M., 2013. WO 2013118125 A1, Composites comprising collagen extracted from sarcophyton sp. coral.

Hollister, S.J., 2009. Scaffold design and manufacturing: from concept to clinic. Adv. Mater. 21, 3330–3342.

Holzapfel, G.A., 2001. Biomechanics of soft tissue. The Handbook of Materials Behavior Models 3, 1049–1063.

Holzapfel, G.A., Sommer, G., Gasser, C.T., Regitnig, P., 2005. Determination of layer-specific mechanical properties of human coronary arteries with nonatherosclerotic intimal thickening and related constitutive modeling. Am. J. Physiol. Heart C 289, H2048–H2058.

Jeong, S.I., Kim, S.Y., Cho, S.K., Chong, M.S., Kim, K.S., H Kim, S.L., Lee, YM, 2007. Tissue-engineered vascular grafts composed of marine collagen and PLGA fibers using pulsatile perfusion bioreactors. Biomaterials 28, 1115–1122.

Kumar, V.A., Caves, J.M., Haller, C.A., Dai, E., Liu, L., Grainger, S., Chaikof, E.L., 2013. Acellular vascular grafts generated from collagen and elastin analogs. Acta Biomater. 9, 8067–8074.

Kumbar, S., James, R., Nukavarapu, S., Laurencin, C., 2008. Electrospun nanofiber scaffolds:engineering soft tissues. Biomed. Mater. 3, 1–15.

Kuo, C.K., Ma, P.X., 2001. Ionically crosslinked alginate hydrogels as scaffolds for tissue engineering: Part 1. Structure, gelation rate and mechanical properties. Biomaterials 22, 511–521.

Lai, J.H., Levenston, M.E., 2010. Meniscus and cartilage exhibit distinct intra-tissue strain distributions under unconfined compression. Osteoarthr. Cartil. 18, 1291–1299.

Lee, K., Mooney, D., 2012. Alginate: properties and biomedical applications. Prog. Polym. Sci. 37, 106–126.

Liao, J., Joyce, E.M., Sacks, M.S., 2008. Effects of decellularization on mechanical and structural proprerties of the porcine aortic valve leaflet. Biomaterials 29, 1065–1074.

McKee, C.T., Last, J.A., Russell, P., Murphy, C.J., 2011. Indentation versus tensile measurements of Young's modulus for soft biological tissues. Tissue Eng. B 17, 155–164.

Parenteau-Bareil, R., Gauvin, R., Berthod, F., 2010. Collagen-based biomaterials for tissue engineering applications. Materials 3, 1863–1887.

Pok, S., Myers, J.D., Madihally, S.V., Jacot, J.G., 2013. A multi-layered scaffold of a chitosan and gelatin hydrogel supported by a pcl core for cardiac tissue engineering. Acta Biomater. 9, 5630–5642.

Rafat, M., Li, F., Fagerholm, P., Lagali, N.S., Watsky, M.A., Rejean Munger, T.M., Griffith, May, 2008. PEG-stabilized carbodiimidecrosslinked collagen–chitosan hydrogels for corneal tissue engineering. Biomaterials 29, 3960–3972.

Ruggiero, F., Exposito, J.Y., Bournat, P., Gruber, V., Perret, S., Comte, J., Olagnier, B., Garrone, R., Theisen, M., 2000. Triple helix assembly and processing of human collagen produced in transgenic tobacco plants. FEBS Lett. 469, 132–136.

Sasson, A., Patchornik, S., Eliasy, R., Robinson, D., Haj-Ali, R., 2012. Hyperelastic mechanical behavior of chitosan hydrogels for nucleus pulposus replacement—experimental testing and constitutive modeling. J. Mech. Behav. Biomed. Mater. 8, 143–153.

Songa, E., Kimb, S.Y., Chunc, T., Byunc, H.-J., Lee, Y.M., 2006. Collagen scaffolds derived from a marine source and their biocompatibility. Biomaterials 26, 2951–2961.

Sutton, M., Wolters, W., Peters, W., Ranson, W., McNeill, S., 1983. Determination of displacements using an improved digital correlation method. Image Vis. Comput. 1, 133–139.

Sutton, M.A., Orteu, J.-J., Schreier, H.W., 2009. Image correlation for shape, motion and deformation measurements. Springer, New York970–978 (doi 10).

Tamayol, A., Akbari, M., Annabi, N., Paul, A., Khademhosseini, A., Juncker, D., 2013. Fiber-based tissue engineering: progress, challenges, and opportunities. Biotechnol. Adv. 31, 669–687.

Telemeco, T., Ayres, C., Bowlin, G., Wnek, G., Boland, E., N Cohen, C.B., Mathews, J, Simpson, DG, 2005. Regulation of cellular infiltration into tissue engineering scaffolds composed of submicron diameter fibrils produced by electrospinning. Acta Biomater. 1, 377–385.

Thorpe, C.T., Birch, H.L., Clegg, P.D., Screen, H.R., 2013. The role of the non-collagenous matrix in tendon function. Int. J. Exp. Pathol. 94, 248–259.

Thorvaldsson, A., Silva-Correia, J., Oliveira, J.M., Reis, R.L., Gatenholm, P., Walkenstrom, P., 2013. Development of nanofiber-reinforced hydrogel scaffolds for nucleus pulposus regeneration by a combination of electro-spinning and spraying technique. J. Appl. Polym. Sci. 128, 1158–1163.

Tremblay, D., Zigras, T., Cartier, R., Leduc, L., Butany, J., Mongrain, R., Leask, R.L., 2009. A comparison of mechanical properties of materials used in aortic arch reconstruction. Ann. Thorac. Surg. 88, 1484–1491.

Wright, L., McKeon-Fischer, K., Cui, Z., Nair, L., Freeman, J., 2012. PDLA/PLLA and PDLA/PCL nanofibers with a chitosan-based hydrogel in composite scaffolds for tissue engineered cartilage, J. Tissue Eng. Regener. Med..

Zeng, Y., Yang, J., Huang, K., Lee, Z., Lee, X., 2001. A comparison of biomechanical properties between human and porcine cornea. J. Biomech. 34, 533–537.

Zeugolis, D.I., Paul, G.R., Attenburrow, G., 2008. Cross-linking of extruded collagen fibers-A biomimetic three-dimensional scaffold for tissue engineering applications. J. Biomed. Mater. Res. A 89A, 895–908.